RSC Advances

ROYAL SOCIETY OF CHEMISTRY

www.rsc.org/advances

Cite this: DOI: 10.1039/c0xx00000x

www.rsc.org/xxxxxx

ARTICLE TYPE

Two nitrogen-rich Ni (II) coordination compounds based on 5,5'-azotetrazole: Synthesis, characterization and effect on thermal decomposition for RDX, HMX and AP†

Dong Chen, Shiliang Huang, Qi Zhang*, Qian Yu, Xiaoqing Zhou, Hongzhen Li* and Jinshan Li*

Received (in XXX, XXX) Xth XXXXXXXXX 20XX, Accepted Xth XXXXXXXXX 20XX
DOI: 10.1039/b000000x

Two novel multiligand coordination complexes of Ni (II), $[Ni(en)_3]AZT{\cdot}THF$ (**1**) (en = ethylene diamine, THF = tetrahydrofuran) and $[Ni(AZT)(pn)_2]_n$. (**2**) (pn = propylene diamine), were prepared from corresponding Ni salt and have been structurally characterized by elemental analysis, Fourier transform infrared spectroscopy and single crystal X-ray diffraction. The results show that both the crystals of **1** and **2** crystallize in the triclinic space group *P*-1. **1** presents a zero-dimensional unit, while **2** exhibits a one-dimensional zigzag chains. Under nitrogen, the thermal decomposition process and the kinetic parameters of the two complexes were studied by TG-DTG and DSC technologies. The non-isothermal kinetic parameters were calculated by the Kissinger's and Ozawa-Doyle's methods. Furthermore, compounds were explored as additives to promote the thermal decomposition of cyclotrimethylene trinitramine (RDX), cyclotetramethylene tetranitramine (HMX) and ammonium perchlorate (AP) by differential scanning calorimetry.

Introduction

Energetic materials nowadays focuses on the synthesis of simple molecules with high energy, high density, high heat resistance and low sensitivity.[1] Compared with traditional energetic materials, nitrogen-rich compounds contain more N-N or C-N groups which hold the higher positive enthalpy formation. Due to their good ability of oxygen balance and capacity to produce more gas under the same mass condition, nitrogen-rich compounds have many advantages in applications such as neotype gas generator, low characteristic signal propellant, smokeless pyrotechnic compound and high explosive.[2-5]

Tetrazoles and their derivatives are widely used in biology and pharmacy because of their similar pH value with carboxylic acid (p*K*a ≈ 4.9), and they attract much attention used as ligands in complex since they are multidentate ligands with many coordination sites which are tend to form multinuclear or multidimensional complexes with a variety of metal ions.[6] As a kind of high nitrogen (84.3%) compound, 5,5'-azotetrazole (AZT) has been studied a lot because it possesses excellent energetic properties compared with other tetrazole derivatives[7] and many salts or complexes of AZT^{2-} have been seen as a class of energetic materials.[8-10] For example, heavy metal salts of Tl, Pb with AZT^{2-} have been used as initiators[11] and complex like copper AZT ($[Cu(NH_3)_4]AZT(H_2O)_2$) is a potential "green" gas generator or additives in solid rockets as low-smoke propellant ingredient[12]. Considering these promising applications, to develop new energetic materials and research the relationship between properties and structures in energetic compounds by virtue of crystal engineering is challenging but necessary.

On the other hand, energetic complexes can be used as burning promoters in solid propellants to broaden their burning rate range, decrease the pressure factor and characteristic signal.[13-15] They affect the thermal decomposition characteristics of common oxidizers like cyclotrimethylene trinitramine (RDX), cyclotetramethylene tetranitramine (HMX) or ammonium perchlorate (AP) and finally influence the combustion behavior of solid propellants.[16,17] Generally, energetic complexes can improve the performances of RDX, HMX or AP by shifting their peak temperature left and increasing their process heat during thermal decomposition,[18] in which complexes can offer certain energy compared with traditional catalysts such as metal oxides. But to our best knowledge, only a few nitrogen-rich complexes have been reported[19-22, 31-34] as promoters and most of them show the limited utility to these propellants.

In this paper, we report on the synthesis and characterization of two nitrogen-rich compounds: $[Ni(en)_3]AZT{\cdot}THF$ (en = ethylene diamine, THF = tetrahydrofuran) and $[Ni(AZT)(pn)_2]_n$. (pn = propylene diamine) The single crystal X-ray experiment reveals the coordination mode of AZT^{2-} with Ni^{2+}. The thermal behavior of materials are determined by TG-DTG and DSC analysis. Moreover, their kinetic parameters of the first exothermic process and the effect towards thermal decomposition of RDX, HMX and AP are explored.

Experimental

General caution: the complex of sodium 5,5'-azotetrazole (SAZT) and its deprotonated anions are potentially explosive and should be handled in small quantities. Appropriate safety precautions should be taken and larger scale synthesis is not recommended.

Materials and instruments

All reagents used for the synthesis were purchased from commercial sources and used without further purification. C, H and N microanalyses were carried out with a Perkin-Elmer 240 elemental analyzer. IR spectra were recorded on KBr discs on a Bruker 6700 spectrophotometer in the 50-3500 cm^{-1} region. Particle size was taken by ZEISS Axio Scope. A1 microscope. Differential scanning calorimetry (DSC) were carried out on DSC823e METTLER TOLEDO with heating rate of 5, 10, 15, 20 ℃/min respectively; thermogravimetric (TG) analysis was

conducted on TGA/SDTA851e METTLER TOLEDO with a heating rate of 10 ℃/min under flowing N_2 at 20 ml/min.

Synthesis of [Ni(ethylenediamine)$_3$]AZT·THF (1)

A: SAZT (0.21 g, 1 mmol), en (70 μl, 1 mmol) and $Ni(NO_3)_2$ (0.145 g, 0.5 mmol) were added to DMSO (2.5 ml) and stirred for 5 min to clarification; B: 1.5 ml DMSO; C: 8 ml THF. Solution A was shifted in the bottom of a clean 1 centimeter diameter glass tube, then B and C was added onto the surface of previous solution slowly in turn to form a diffusion system. Light brown crystals were obtained in the diffused part after several days. (Yield: 56%, based on Ni). Anal. Calcd. (%) : C, 31.09; H, 4.32; N, 48.36. Found: C, 31.02; H, 4.28; N, 48.31. IR spectrum (KBr, cm^{-1}): 3305 (s), 2939 (m), 2235 (w), 1591 (s), 1388 (s), 1268 (w), 1018 (s), 873 (w), 728 (m), 692 (m).

Synthesis of [Ni(AZT)(propylene diamine)$_2$]$_n$ (2)

A: Propane diamine (85 μl, 1 mmol) was added to a solution of $Ni(NO_3)_2$ (0.145 g, 0.5 mmol) in water(3 ml) and stirred for 5 min. B: 2 ml water and methanol mixture with the same-size ratio. C: 0.105 g (0.5 mmol) SAZT in 5 ml methanol was stirred to clarification. Solution A was shifted in the bottom of a clean 1 centimeter diameter glass tube, then B and C was added onto the surface of previous solution slowly in turn to form a diffusion system. Brown crystals were obtained in the diffused part after several days. (Yield: 49%, based on Ni). Anal. Calcd. (%) : C, 26.38; H, 5.49; N, 53.85. Found: C, 26.32; H, 5.44; N, 53.71. IR spectrum (KBr, cm^{-1}): 3436 (w), 3255 (m), 2946 (s), 2888 (s), 2238 (w), 2420 (w), 1583 (s), 1463 (m), 1280 (s), 1157 (s), 4908 (s), 730 (s).

X-Ray crystallography and data collection

The crystals were filtered from the solution and immediately coated with a hydrocarbon oil on the microscope slide. Suitable crystals were mounted on glass fibers with silicone grease and placed in a Bruker Smart APEX(II) area detector using graphite monochromated Mo Kα radiation (λ = 0.71073Å) at 140(2) K. Their structures were solved by direct methods and successive Fourier difference syntheses using the SHELXTL software suite. Hydrogen atoms were added theoretically and were riding on their parent atoms. Crystallographic data were deposited in the Cambridge Crystallographic Database Centre: CCDC-1045384 for **1**, 1045385 for **2**. Other details of crystal data, data collection parameters and refinement statistics are given in Table 1.

Table 1. Crystal data and structure refinement for **1** and **2**

Compound	1	2
Empirical formula	$NiC_{12}H_{32}ON_{16}$	$NiC_8H_{20}N_{14}$
Formula weight	475.23	371.09
Crystal system	Triclinic	Triclinic
Space group	*P*-1	*P*-1
a/Å	9.439(5)	6.7483(8)
b/Å	10.414(4)	8.2141(9)
c/Å	12.275(5)	8.2854(9)
α (°)	103.66(1)	113.25(1)
β (°)	109.22(0)	112.49(1)
γ (°)	99.02(1)	97.53(1)
V (Å^3)	1070.4(8)	367.73(7)
Z	2	1
Dc/g cm^{-3}	1.474	1.676
F(000)	504	194
μ / mm^{-1}	0.948	1.346
R_1 (all data)	0.0672	0.0561
wR_2 (all data)	0.1823	0.1884

Results and discussion

Description of structures

The crystal structure of compound [Ni(en)$_3$]AZT·THF (1). Single-crystal analysis shows the complex crystallizes in triclinic space group *P*-1. The atomic labeling diagram of [Ni(en)$_3$]AZT·THF is show in Fig. 1(a). Each unit of 1 consists one Ni^{2+} ion, three en ligand molecules, two half trans-AZT^{2-} ions and one free THF molecule (There are no strong connections between THF and any other atom, its disordered form is represented as is in Fig. 1(a).). The central Ni^{2+} ion is hexa-coordinated with six nitrogen atoms from three en ligand molecules to form the slightly distorted [NiN_6] octahedra. As is listed in Table 2 and Table 3, the Ni-N bond lengths lie in the range 2.116(4)-2.135(4)Å, and the trans-AZT^{2-} anions act as counter ions to maintain charge balance. The axial bond angles of N(4)-Ni(1)-N(1), N(2)-Ni(1)-N(5), N(6)-Ni(1)-N(3) are 171.46°, 171.34°, 172.02° respectively, which slightly deviate from linearity of 180°.

As is showed in Fig. 1(a), the en ligand acts as a bidentate ligand forming with the central metal ion into a disordered, five-member chelate ring. The dihedral angles between the rings are almost 90°, leading to the least steric hindrance and the stable space structure. The trans-AZT ions stack along the a and c axes to build crystal, and neighbouring separated interplanar distance of tetrazole rings is about 9Å. Two THF molecules are caged in cavity constructed by trans-AZT ions. The complicated 3D structure of **1** viewed along the y axis is shown in Fig. 1(b). There are hydrogen bonds N-H···N exist between AZT^{2-} and ethylenediamine in crystal which stabilize the complex structure, their bonds length is between 3.05-3.10Å (Table. S1, ESI†) (Fig. 1(c)). Intermolecular hydrogen bonds in compound link lignds and AZT^{2-} ions molecules into a three-dimensional network structure.

Table 2. Main bond length (Å) for **[Ni(en)$_3$]AZT·THF** and **[Ni(AZT)(pn)$_2$]$_n$**

[Ni(en)$_3$]AZT·THF			
Ni(1)-N(6)	2.116(4)	Ni(1)-N(4)	2.131(4)
Ni(1)-N(3)	2.118(4)	Ni(1)-N(1)	2.135(4)
Ni(1)-N(2)	2.126(4)	Ni(1)-N(5)	2.134(4)
[Ni(AZT)(pn)$_2$]$_n$			
Ni(1)-N(5)	2.1513	Ni(1)-N(18)	2.1258
Ni(1)-N(11)	2.1591	Ni(1)-N(21)	2.1525
Ni(1)-N(14)	2.1020	Ni(1)-N(22)	2.1614

Table 3. Main angle (°) for **[Ni(en)$_3$]AZT·THF** and **[Ni(AZT)(pn)$_2$]$_n$**

[Ni(en)$_3$]AZT·THF			
N(6)-Ni(1)-N(3)	172.02(15)	N(2)-Ni(1)-N(1)	82.28(15)
N(6)-Ni(1)-N(2)	92.53(16)	N(4)-Ni(1)-N(1)	171.46(15)
N(3)-Ni(1)-N(2)	93.45(16)	N(6)-Ni(1)-N(5)	82.31(16)
N(6)-Ni(1)-N(4)	91.95(16)	N(3)-Ni(1)-N(5)	92.37(15)
N(3)-Ni(1)-N(4)	82.62(15)	N(2)-Ni(1)-N(5)	171.34(16)
N(2)-Ni(1)-N(4)	91.51(15)	N(4)-Ni(1)-N(5)	95.58(15)
N(6)-Ni(1)-N(1)	94.18(16)	N(1)-Ni(1)-N(5)	91.13(15)
N(3)-Ni(1)-N(1)	91.85(16)		
[Ni(AZT)(pn)$_2$]$_n$			
N(14)-Ni(1)-N(18)	172.02(15)	N(18)-Ni(1)-N(11)	91.85(16)
N(14)-Ni(1)-N(5)	92.53(16)	N(18)-Ni(1)-N(22)	82.28(15)
N(14)-Ni(1)-N(21)	93.45(16)	N(5)-Ni(1)-N(21)	171.46(15)
N(14)-Ni(1)-N(11)	91.95(16)	N(5)-Ni(1)-N(11)	82.31(16)

N(14)-Ni(1)-N(22)	82.62(15)	N(5)-Ni(1)-N(22)	92.37(15)
N(18)-Ni(1)-N(5)	91.51(15)	N(21)-Ni(1)-N(11)	171.34(16)
N(18)-Ni(1)-N(21)	94.18(16)	N(21)-Ni(1)-N(22)	95.58(15)

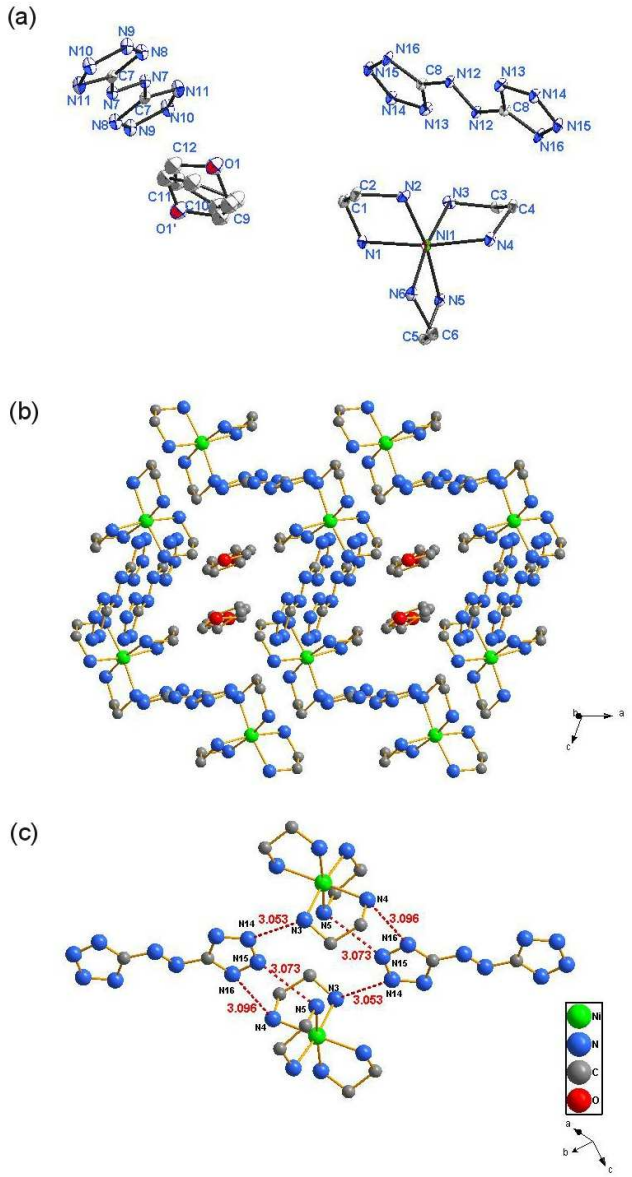

Fig. 1. (a) ORTEP view (30 thermal ellipsoids) of **1**, (b) The complicated 3D structure of **1** viewed along the y axis, (c) the N-H···N hydrogen bonding generated in **1**. Hydrogen atoms are omitted for clarify.

The crystal structure of compound $[Ni(AZT)(pn)_2]_n$ (2).

Complex $[Ni(AZT)(pn)_2]_n$ crystallizes in triclinic space group *P*-1. The atomic labeling diagram of $[Ni(AZT)(pn)_2]_n$ is show in Fig. 2(a). Each unit of $[Ni(AZT)(pn)_2]_n$ consists one Ni^{2+} ion, two pn ligand molecules, two half trans-AZT^{2-} ions. The central Ni^{2+} ion is hexa-coordinated with six nitrogen atoms to form the slightly distorted $[NiN_6]$ octahedra, in which the two N atoms come from two AZT^{2-} ions and other four N atoms are from two en molecules. As is listed in Table 2 and Table 3, the Ni-N bonds length with AZT^{2-} ion in Ni(1)-N(5), Ni(1)-N(11) are 2.1513Å and 2.1591Å respectively. And Ni-N bonds length with pn molecules in Ni(1)-N(14), Ni(1)-N(18), Ni(1)-N(21), Ni(1)-N(22) are between 2.10Å-2.16Å. The trans-AZT^{2-} anions act as counter ions to maintain charge balance. The axial bond angles of N(5)-Ni(1)-N(11), N(14)-Ni(1)-N(22), N(18)-Ni(1)-N(21) are 178.89°, 178.91°, 177.35° respectively, which slightly deviate from linearity of 180°.

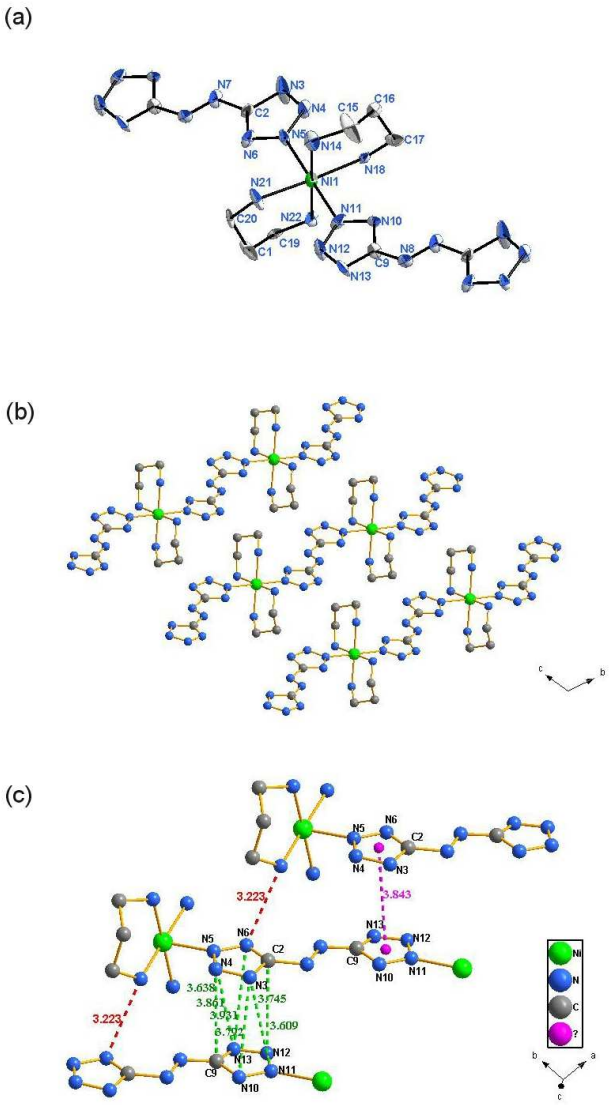

Fig. 2. (a) ORTEP view (30 thermal ellipsoids) of **2**, (b) The 3D supramolecular structure of **2** viewing long a axis, (c) The face-to-face tetrazolate anion alignment showing the π-π stacking interaction and the N-H···N hydrogen bonding generated in **2**. Hydrogen atoms are omitted for clarify.

As is showed in Fig. 2(a), the pn ligand acts as a bidentate ligand forming with the central metal ion into a disordered, six-member chelate ring. The dihedral angles between the pn rings and the AZT^{2-} plane are almost 90°, leading to the least steric hindrance and the stable space structure. The AZT^{2-} ion ligand acts as a bidentate ligand and behaves a μ_2 bridging model with N(5) and N(11) coordinating to two different Ni^{2+} ions, resulting in a 1D chain structure(Fig. 2(b)). Compound **2** has the similar framework with $[Ni(en)_2(AZT)_2](en)_2{\cdot}H_2O$,[23] but here we use pn which possesses longer carbon chain and more flexibility than en to construct new complex. The neighbouring separated interplanar distance of tetrazole rings is about 3.843Å, it shows the face-to-face anion-anion π^--π^- stacking interactions(Fig. 2(c)).

There are N-H···N hydrogen bonds exist between AZT^{2-} and propylenediamine in crystal and their bonds length is 3.223Å (Table. S2, ESI†). Intermolecular π^{-}-π^{-} stacking interactions and hydrogen bonds in compound link 1D chains into a three-dimensional network structure.

Thermal decomposition

The DSC and TG-DTG curves with the linear heating rate of 10 □/min under nitrogen atmosphere are shown in Fig. 3 and Fig. 4 to demonstrate the thermal decomposition processes of compounds **1** and **2**. In the DSC curves, there is one intense exothermic process from 206 to 278 □ peaking at 246 □ for **1** and one intense exothermic process from 223 to 274 □ peaking at 247 □ for **2**, which are identical to the peaks temperature that appeared on the DTG curves. The relevant exothermic enthalpy change of **1** is 170.8 kJ/mol and for **2** is 144 kJ/mol. There for, these metal-organic crystals contain the AZT ligand are thermally stable enough to be energetic materials[24]. Corresponding to these exothermic processes, a fast mass lose around 246 □ can be seen from Fig.3, 32.14% and 40.62% for 1 and 2 respectively. It indicates the collapses of the crystal structures related to the nitrogen-rich groups AZT. After the fast exothermic decomposition process, there is a persistent exothermic reaction slower than the former process till to the end of the test. The observed mass loss value is 36.9% for **1** and 31.6% for **2**. This is related to the following partial decomposition of the residual of compounds **1** and **2**. In the infrared spectrum of the final decomposed residues of 1 and 2 at 700 □, the characteristic absorption bands of $[Ni(en)_3]AZT{\cdot}THF$ and $[Ni(AZT)(pn)_2]_n$ have disappeared, the existence of the absorption peak around 436 cm^{-1} in both residues proves the final decomposed residue is mainly NiO (Fig. S1-3, ESI†).

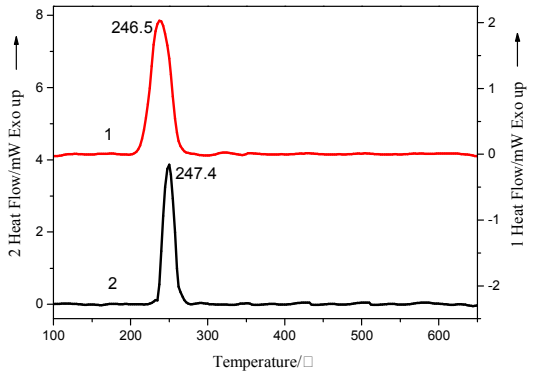

Fig. 3 DSC curves of compounds **1** and **2** at a heating rate of 10K/min.

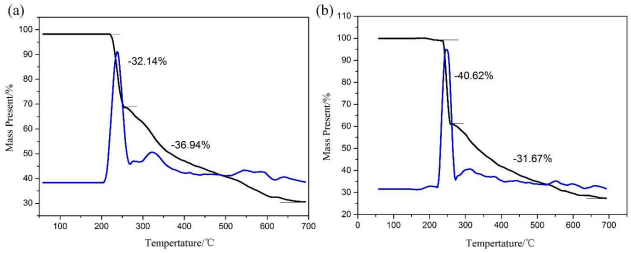

Fig. 4 TG-DTG curves of compounds **1** (a) and **2** (b) at a heating rate of 10K/min.

Non-isothermal kinetics analysis

Kissinger's[25] and Ozawa's methods[26,27] were used to determine the kinetics parameters based on the first exothermic peaks temperature measured from DSC curves with four different heating rates (5, 10, 15, 20 □/min). The Kissinger (1) and Ozawa-Doyle (2) equations are as follows:

$$\ln\frac{\beta}{T_p^{\,2}} = \ln\left(\frac{RA}{E}\right) - \frac{E}{R}\cdot\frac{1}{T_p} \quad (1)$$

$$\log\beta + \frac{0.4567E}{RT_p} = C \quad (2)$$

Where T_p is the peak temperature; A is the pre-exponential factor; E is the apparent activation energy; R is the gas constant (8.314 $JK^{-1}mol^{-1}$). The calculated results using both methods include linear correlation coefficient r_k and r_o are shown in Table 4 (subscripts K and O represent calculation results of Kissinger's method and Ozawa-Doyle's method). Accordingly, the Arrhenius equations for $[Ni(en)_3]AZT{\cdot}THF$ and $[Ni(AZT)(pn)_2]_n$ can be expressed as Equations (3) and (4) respectively:

$$\ln k = 46.69 - 202.8\times10^3/(RT) \quad (3)$$

$$\ln k = 49.65 - 218.8\times10^3/(RT) \quad (4)$$

The result shows that the activation energy of $[Ni(AZT)(pn)_2]_n$ is higher than that of $[Ni(en)_3]AZT{\cdot}THF$. These equations can be used to estimate the rate constants for the thermal decomposition processes of compounds **1** or **2** and predict their thermal decomposition mechanisms.

Table 4 The calculated kinetic parameters for the first exothermic decomposition processes of **$[Ni(en)_3]AZT{\cdot}THF$** and **$[Ni(AZT)(pn)_2]_n$**

β(k/min)	T_p[a](k)	E_K[b](kJ/mol)	r_K[b]	lnA_K[b]	E_O[c](kJ/mol)	r_O[c]
$[Ni(en)_3]AZT{\cdot}THF$						
5	512.85	202.8	0.9992	46.69	200.0	0.9838
10	520.65					
15	524.55					
20	527.75					
$[Ni(AZT)(pn)_2]_n$						
5	513.25	218.8	0.9944	49.65	232.6	0.9998
10	519.65					
15	523.75					
20	526.35					

[a] T_p: maximum peak temperature.
[b] Subscript K: Kissinger's method.
[c] Subscript O: Ozawa-Doyle's method.

Effects on thermal decomposition of RDX, HMX and AP

Compound **1** and **2** are explored as promoters to the thermal decomposition of cyclotrimethylene trinitramine (RDX), cyclotetramethylene tetranitramine (HMX) and ammonium perchlorate (AP) which are the important compounds of composite solid propellants. Compound **1** or **2** were mixed with RDX, HMX or AP at a mass ratio of 1:3 (25%) respectively, all compounds should be handled in small quantity (within 10 mg) and ground gently in the agate mortar to the good uniformity, appropriate safety precautions should be taken. Particle size of RDX, HMX is about 10 μm and the average particle size of AP, compound **1** and compound **2** is around 30 μm. The performance of compounds on these three energetic materials are investigated by DSC measurement with a heating rate of 10 □/min in N_2 atmosphere between 50-400 □ for RDX and HMX, 50-500 □ for AP, using Al_2O_3 as reference. It should be noticed that a total mass used is less than 1mg for all runs.

Fig. 5 shows the DSC curves of RDX and the mixtures of RDX with compounds **1** or **2**. The endothermic peak of RDX at 208 □ is ascribed to the melting endotherm process of RDX and the exothermic peak at 248 □ is due to the complete decomposition of RDX into volatile products, corresponding to the heat of 1282.8 J/g. From Fig. 5b and c, we can see that the melt peak has disappeared and there is only one exothermic peak in both two

curves. It is obvious that the peaks temperature of **1**/RDX (223 ℃) and **2**/RDX (204 ℃) is much lower than that of pure RDX, has decreased by 44 ℃ and 25 ℃ respectively, meanwhile the decomposition heat increases to 1551.56 J/g for **2**/RDX and 1610.1 J/g for **1**/RDX, increased by 21% and 26% respectively.

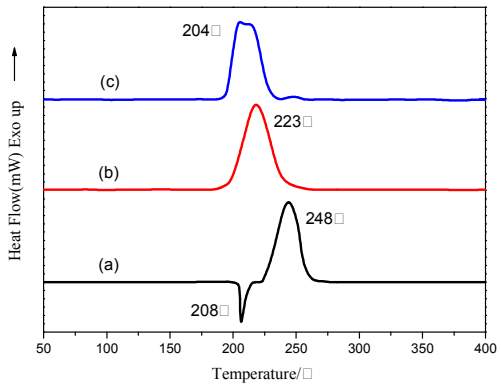

Fig. 5 DSC curves for RDX (a), **1**+RDX (b) and **2**+RDX (c).

The DSC curves of HMX and the mixtures of HMX with compounds **1** or **2** can be seen in Fig. 6. The only exothermic peak at 289 ℃ is due to the complete decomposition of HMX with the heat of 1279.5 J/g. From Fig. 6c, we can see that the peak temperature of **2**/HMX (251 ℃) is much lower (decreased by 38 ℃) than that of pure HMX while its decomposition heat increases to 1495.2 J/g, increased by 17%. The sharp exothermic peak indicates a rapid decomposition process. The peak temperature of **1**/HMX is 285 ℃ and its decomposition heat is 1520.2 J/g, increased by 19%.

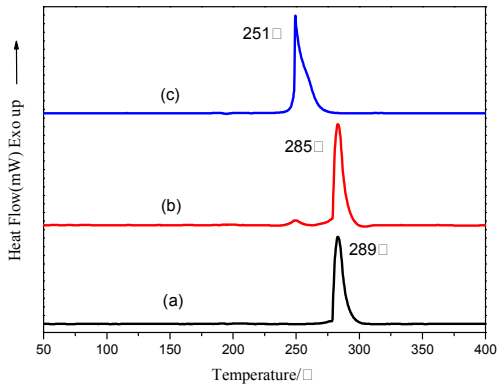

Fig. 6 DSC curves for HMX (a), **1**+HMX (b) and **2**+HMX (c).

As is shown in Fig. 7, the DSC curves of AP and the mixtures of AP with compounds **1** or **2** are explored. The endothermic peak of AP in Fig. 7a at 244 ℃ is due to its crystal transformation from orthorhombic to cubic phase[28]. The exothermic peaks at 298 ℃ and 420 ℃ is attributed to the partial decomposition to form some intermediate product and then complete decomposition of AP[29,30], corresponding to the heat of 206.1 J/g and 133 J/g respectively in our tests. From Fig. 7b and c, we can see that the compounds have no significant impact on the phase transition, but there are some significant changes in the decomposition patterns. The first exothermic peak in pure AP has declined from 298 ℃ to 290 ℃ and 285 ℃ for **2**/AP and **1**/AP respectively, and their decomposition heat has no apparent distinction with pure AP. It is apparent that the second exothermic peaks temperature of **1**/AP (362 ℃) and **2**/AP (362.5 ℃) is much lower than that of pure AP (420 ℃), has decreased by 58 ℃ for both compounds and the corresponding decomposition heat has fiercely increased to 532.5 J/g for **2**/AP and 706.1 J/g for **1**/AP, increased by 399 J/g (300%) and 573 J/g (430%) respectively. Control experiments have been carried out in which the mass ratio of 25% has been decreased to 15%, but the result is not as good as before (Fig. S7-9, ESI†). There should exist a best mass ratio area in different mixture systems, that is the optimum value for resulting the highest temperature drop and process heat at the same time.

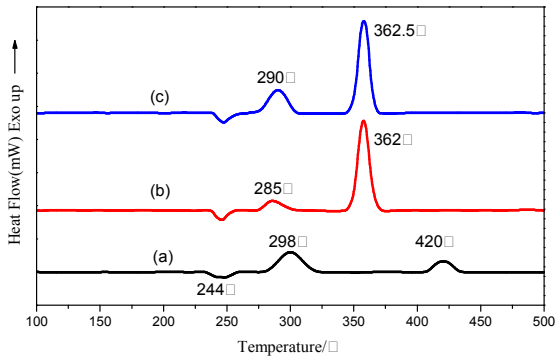

Fig. 7 DSC curves for AP (a), **1**+AP (b) and **2**+AP (c).

In conclusion, both complexes show good effect on the thermal decomposition of RDX, HMX and AP. DSC experiments reveal that compound **1** and **2** accelerate the decomposition of RDX, HMX and AP. The highest drop value for mixture systems of **2**/RDX, **2**/HMX is 44 ℃ and 38 ℃ respectively, both compounds have decreased the decomposition temperature of AP by 58 ℃. The exothermic quantity of **1**/RDX, **2**/RDX, **1**/AP and **2**/AP has increased by 323 J/g, 269 J/g, 573 J/g and 399 J/g respectively. It can be inferred that in the mixture systems of **1**/RDX, **2**/RDX, **1**/HMX, **2**/HMX, **1**/AP and **2**/AP, the compounds decompose and release much heat itself which enhance the total process heat of the mixtures. In terms of the catalytic mechanism, we consider that the formation of metal oxides at molecular level on energetic materials surface could enhance their effect further[18]. It should be noticed that compound **2** has more remarkable effect on both RDX and HMX than compound **1**.

In order to evaluate the performance of compounds 1 and **2** in promoting the thermal decomposition of propellants, we compared their effect on temperature drop with some previously reported typical data of nitrogen-rich complexes[18,31-34] (Fig. S10-14, ESI†) in Fig. 8, as peak temperature is more stable and reliable during the DSC experiment. All mixtures are mixed and tested in the same way like what mentioned before.

It is obvious that compound **2** has excellent effect on all these three propellants and leads to the highest temperature drop in mixtures of RDX (44 ℃) and HMX (38 ℃). Compound **1** has good performance in mixtures of RDX (25 ℃) and AP (57 ℃) but brings the least temperature drop (4 ℃) with HMX. Although $[Pb_2(ANPyO)_2(NMP)\cdot NMP]_n$ behaves good in mixture with AP (54 ℃), it decreases decomposition temperature of RDX only by 2 ℃. Complex $[Co(ANPyO)_3]\cdot 3DMF$ leads to the considerable temperature drop around 60 ℃ in AP mixture and other complexes have moderate effect on decomposing propellants which slightly decrease their decomposition temperature.

Therefore, compound **2** presents extensive utility to these common oxidizers.

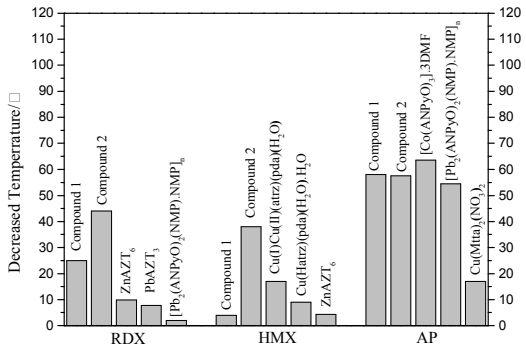

Fig. 8 Decreased temperature in the mixture systems of several typical nitrogen-rich complexes and common oxidizers in propellants at a mass ratio of 1:3.

Considering both compound **1** and **2** include metal Ni^{2+} part and AZT^{2-} part, control experiments were conducted using sodium 5,5'-azotetrazole (SAZT) and tris(ethylenediamine) nickel(II) sulfate ($Ni(en)_3SO_4$) to evaluate their importance to the thermal decomposition of propellants. $Ni(en)_3SO_4$ was synthesized according to literature[35] (Fig. S4, ESI†), SAZT and $Ni(en)_3SO_4$ were mixed with RDX, HMX or AP at the corresponding mole ratio converted from former mixtures which mixed with the 1:3 mass ratio. Here DSC curves of RDX with SAZT or $Ni(en)_3SO_4$ were taken as example. As is shown in Fig. 9b and c, the peak temperature of SAZT/RDX (238 □) and $Ni(en)_3SO_4$/RDX (208 □) is lower than that of the pure RDX, meanwhile their thermal decomposition heat is 1288.52 J/g and 715.9 J/g, respectively. So the decomposition temperature of $Ni(en)_3SO_4$/RDX is much lower than that of SAZT/RDX but the system of SAZT/RDX holds much more decomposition heat than that of $Ni(en)_3SO_4$/RDX. The similar results can be also obtained from other experiments with HMX and AP (Fig. S5-6, ESI†). Moreover, compound **1** and **2** still keep their advantages as promoters when compared with the results of the control experiments, since they can lead to the considerable temperature drop and the highest process heat (Fig. 5).

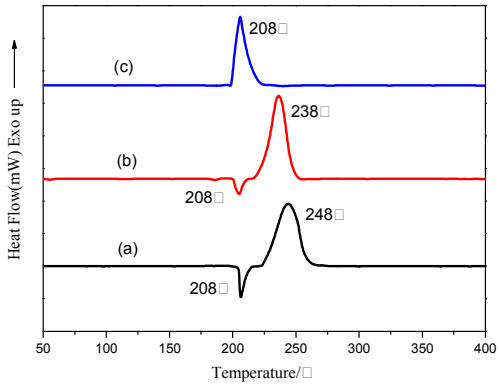

Fig.9 DSC curves for RDX (a), SAZT+RDX (b) and $Ni(en)_3SO_4$+RDX (c).

These consistent experimental results indicate that the metal Ni^{2+} part and AZT^{2-} part in two compounds represent different importance on the thermal decomposition of propellants. For metal Ni^{2+} part, formation of metal oxides at molecular level on energetic materials surface have more important effects on shifting their peak temperature left, just like other reported metallic oxide catalysts; for AZT^{2-} part, as a kind of high-nitrogen compound itself, it has more important effect on increasing their process heat during thermal decomposition. So these two parts could enhance their effect further when they are in the same compound through chemical bonds. It can be inferred that this kind of positive synergistic function exists not only in compound **1** and **2** but also in all energetic complexes. We think there exists more complicated mechanism during the thermal decomposition of mixture systems. Further investigation is currently being processed.

Conclusions

In summary, we have synthesized two novel multiligand coordination complexes of nickel(II): $[Ni(en)_3]AZT{\cdot}THF$ (**1**) and $[Ni(AZT)(pn)_2]_n$. (**2**), which have been characterized using a variety of techniques such as elemental analyses, Fourier transform infrared spectroscopy, TG-DSC studies, and single crystal X-ray diffraction. X-ray single crystal structure analysis indicate that both the crystals of **1** and **2** crystallize in the triclinic space group *P*-1. **1** and **2** present zero-dimensional unit and one-dimensional zigzag chains respectively. TG-DTG and DSC studies indicate there is one intense exothermic decomposition for both **1** and **2** around 247 □. The activation energy of the first exothermic process of compound **2** is a little higher than that of the compound **1** and is shown in the Kissinger's and Ozawa-Doyle's methods. DSC experiments reveal that both complexes show prominent effect on the thermal decomposition of RDX, HMX and AP. The decomposition of RDX, HMX and AP has been accelerated by two compounds. In the mixture systems of **1**/RDX, **2**/RDX, **1**/HMX, **2**/HMX, **1**/AP and **2**/AP, the compounds decompose and release much heat itself which enhance the total process heat of the mixtures. Control experiments with $Ni(en)_3SO_4$ and SAZT indicate that the metal Ni^{2+} part in complex mainly contributes to temperature drop while the AZT^{2-} part can offer more decomposition heat. This kind of positive synergistic function could exist not only in compound **1** and **2** but also in all energetic complexes. It should be noticed that compound **2** presents more extensive utility to these common oxidizers than compound **1**. Both compounds **1** and **2** could be useful promoters in propellants.

Acknowledgements

This work was supported by the National Natural Science Foundation (No.21302176 and 21172203) and the Development Foundation of CAEP (No.2013B0302038 and No.2013B0302042).

Notes and references

[a] *Institute of Chemical Materials, China Academy of Engineering Physics, Mianyang 621900, China;*
**Address for correspondence. Email: jackzhang531@gmail.com*

† Electronic Supplementary Information (ESI) available: Bond lengths and angles for **1** and **2**; Fig. S1-S9. See DOI: 10.1039/b000000x/

‡ Footnotes should appear here. These might include comments relevant to but not central to the matter under discussion, limited experimental and spectral data, and crystallographic data.

[1] G. Singh and S. P. Felix, *J. Hazard. Mater*. **2002**, 90(1), 1-17.
[2] M. A. Hiskey, D. E. Chavez and D. Naud, US, 6458227. **2002-03-13**.
[3] S. Fallis, R. Reed and Y. C. Lu, Proceedings of Halon Options

Technical Working Conference, **2000**.
[4] D. E. Chavez, M. A. Hiskey and R. D. Gilardi, *Angew. Chem., Int. Ed.* **2000**, 112(10), 1861-1863.
[5] M. A. Hiskey, D. E. Chavez and D. Naud, US, 6342587. **2002-04-15**.
[6] M. Paik. Suh, H. J. Park, T. K. Prasad and D.-W. Lim, *Chem. Rev.* **2012**, 112, 782.
[7] G. Steinhauser and T. M. Klapötke, *Angew. Chem., Int. Ed.* **2008**, 47, 2-20.
[8] A. Hammerl, T. M. Klapötke, H. Nöth and M. Warchhold, *Inorg. Chem.* **2001**, 40, 3570-3575.
[9] A. Hammerl, H. Gerhard, T. M. Klapötke, P. Mayer, H. Nöth, H. Piotrowski and M. Warchhold, *Eur. J. Inorg. Chem.* **2002**, 834-845.
[10] S. Gurdip, P. Rishikesh and F. Roland, *J. Hazard. Mater.* **2005**, 118: 75-78.
[11] (a) M. M. Chaudhri, *Nature,* **1976**, 263, 121–122. (b) R. J. Spear and P. P. Elischer, *Aust. J. Chem.* **1982**, 35, 1–13. (c) V. K. Mohan and T. B. Tang, *J. Chem. Phys*. **1983**, 79, 4271–4278.
[12] G. H. Tao, B. Twamley and J. M. Shreeve, *Inorg. Chem.* **2009**, 48. 9918-9923.
[13] T. L. Zhang, R. Z. Hu and F. P. Li, *Acta Chimica Sinica*, **1994**, 52(6), 545-550.
[14] X. Z. Fan, J. Z. Li and L. Y. Zhang, *Chinese Journal of Energetic Materials*, **2007**, 15(4), 316-319.
[15] W. A. Trzcinski, S. Cudzilo and J. Paszula, *Propellants Explosive Pyrotechnics*, **2007**, 32, 502-506.
[16] M. Friedrich, J. C. Galves-Ruiz, T. M. Klapotke, P. Mayer, B. Weber and J. J. Weigand, BTA copper complexes, *Inorg. Chem.* **2005**, 44, 8044-8052.
[17] D. E. G. Jones, K. Armstrong, T. Parekunnel and Q. S. M. Kwok, *J. Therm. Anal. Calorim.* **2006**, 86, 8-1682.
[18] Q. Yang, S. Chen, G. Xie and S. Gao, *J. Hazard. Mater.* **2011**, 197, 199-203.
[19] Y. F. Liu, Y. Chen and L. Shi, *Propellants Explosive Pyrotechnics*, **2012**,37,69-73.
[20] H. B. Liu, Q. Z. Jiao and Y. Zhao, *Journal of Alloys and Compounds*, **2010**, 496(1-2), 317-323.
[21] Z. Q. Xia, S. P. Chen and Q. Wei, *Journal of Solid Chemistry*, **2011**, 184(7), 1777-1783.
[22] H. Z. Duan, X. Y. Lin and G. P. Liu, *Chinese Journal of Chemical Engineering*, **2008**, 16(2), 325-328.
[23] J. Lin, Y. Qin, W. Chen, M. Yang, A. Zhou, W. Dong and C. Tian, *CrystEngComm*, **2012**, 14, 2779.
[24] (a) M. H. V. Huynh, M. A. Hiskey, T. J. Meyer and M. Wetzler, *Proc. Natl. Acad. Sci. U.S.A.* **2006**, 103, 5409–5412. (b) M. H. V. Huynh, M. D. Coburn, T. J. Meyer and M. Wetzler, *Proc. Natl. Acad. Sci. U.S.A.* **2006**, 103, 10322–10327.
[25] H. E. Kissinger, *Anal. Chem.*, **1957**, 29, 1702-1706.
[26] T. Ozawa, *Bull. Chem. Soc. Jpn.*, **1965**, 38, 1881-1885.
[27] C. D. Doyle, *J. Appl. Polym. Sci.*, **1961**, 5, 285-292.
[28] J. A. Creighton and D. G. Eadon, *J. Chem. Soc. Faraday Trans*. **1991**, 87, 3881 - 3891.
[29] W. A. Rosser and S. H. Inami, *Combust. Flame,* **1968**, 12(5), 427 - 435.
[30] P. W. M. Jacobsete and G. S. Pearson, *Combust. Flame,* **1969**, 13(4) 419 - 430.
[31] B. Jiao, Z. Yan and S. Chen, *Chinese Journal of Explosives & Propellants*, **2012**, 35(3), 52-55.
[32] Q. Yang, S. Chen, G. Xie and S. Gao, *Journal of Coordination Chemistry*, **2012**, 65(14), 2584-2592.
[33] J. Liu, Z. Liu, J. Cheng and D. Fang, *Journal of Solid Chemistry*, **2013**, 200, 43-48.
[34] J. Wei, D. Zhang, Q. Yang, S. Chen and S. Gao, *Inorganic Chemistry Communication*, **2013**, 30, 13-16.
[35] M. Haque, C. N. Caughlan and K. Emerson, *Inorg. Chem*. **1970**, 9(11), 2421.